SPIE; SAN DIEGO Vol 509
1985
p 76-92

Fine guidance sensor design optimization for space infrared telescope facility (SIRTF)

S. B. Grossman

Lockheed Missiles & Space Company, Inc.
Electro-Optics Laboratory, O/95-40, B/201
3251 Hanover St., Palo Alto, California 94304

Abstract

A number of applications require the precise tracking or position estimation of an object unresolved in the system optics. This paper evaluates several (NxN) centroid-like interpolation algorithms (N=2,3,4,5) designed to make these estimates to subpixel accuracy. Analytic and Monte Carlo results are presented. The tracking sensor examined was a staring mosaic array (100% coverage assumed) of detectors assumed to be device-noise (e.g., CCD noise) limited. The detector size was varied parametrically to determine the relative performance and to obtain the optimum configuration. The optics blur spot was assumed Gaussian. The sources of error considered to affect the algorithm performance were the systematic algorithm bias (or positional error), the random noise (or jitter error), and the postcalibration residual detector responsivity nonuniformities. The results were applied to the design of the SIRTF Fine Guidance Sensor.

Track accuracy improves with signal-to-noise ratio (SNR), until limited by algorithm inaccuracies or focal-plane nonuniformity. But blur spot distortion has significant impact on algorithm performance.

Among the algorithms tested, the relative SNR performance improved as N decreased. However, extreme sensitivity to algorithm bias error limited the use of the (2x2) algorithm to cases with positional requirements $\geq$ L/25 (even with correction). The (3x3) algorithm is then optimum for positional requirements $\geq$ L/100 (with correction). Higher (NxN) algorithms are required for greater positional accuracy.

Introduction

Mosaic focal plane arrays are particularly suitable for point-source position estimation in astronomical, tracking, surveillance, alignment and optical wavefront sensors. Often the sensor focal plane is designed primarily or solely for best individual detector sensitivity or for good performance with one specific position estimation (interpolation) algorithm. This work reports the results of designing a mosaic star sensor for SIRTF and optimizing the track (interpolation) algorithms for the best accuracy in spot position determination and least relative sensitivity to aberrations or optical distortions. It includes supporting Monte Carlo results.

The performance of several algorithms for point-source position estimation using a mosaic array of detectors was quantified for various noise sources and blur spot distortions, with detector size as a variable. The algorithm performance analysis was then confirmed with Monte Carlo simulations.

The tracking problem undertaken will first be described. The sources of error will then be defined and quantified. The results of parametric variations of the tracking detector size and blur spot shape will be given. The confirming results of Monte Carlo simulation will then be reported, followed by a discussion of the implication of the work done for optimum SIRTF tracker focal-plane design.

Star trackers are often star imagers with visible quadrant cell or mosaic focal plane arrays. The quadrant cell has limited tracking dynamic range and can be operated essentially only as a null sensor. It, thus, requires that the object being observed by the telescope also be a suitable star-like object for tracking by the star sensor. This is not always the case as for extended visible sources or for many infrared sources of interest to SIRTF. The use of visible mosaic arrays in a staring star sensor significantly expands the tracking dynamic range and allows the use of off-axis guide stars for tracking infrared or extended sources.

These types of designs have been considered in previous development work in the SIRTF program. Work on this problem has been reported, much of it in connection with the design of star sensors with CCD-based readouts. Cox[1] performed Monte Carlo studies of point-source image tracking three-point algorithms as a function of signal-to-noise ratio (SNR) (assuming that the limiting noise was that of the CCD), focal-plane fill factor, and the ratio of spot size to detector size. The present paper provides analytic and Monte

Carlo simulations for several different centroid algorithms, allowing a comparison of relative SNR performance. Cassidy and Kaplan[2] have emphasized the importance of sensor calibration: unless the optics distortion and the focal-plane nonuniformities can be removed from the data, the desired spot position accuracies often cannot be obtained. Dennison and Stanton[3] and Salomon and Glavich[4] have also considered the adverse effects of optical distortion on position estimates for a visible star sensor (these papers also refer to previous Jet Propulsion Laboratory studies). The present paper analyzes the various sampling errors (algorithm bias errors) inherent in the various interpolation routines. Though they can be suppressed with correction functions, the efficiency of the correction varies with the choice of algorithm. Furthermore, the various algorithm sensitivities to optical (blur spot) distortion is also compared. We also evaluated the limitation placed on performance by focal-plane nonuniformities, thus quantifying the calibration accuracy requirements.

This analysis allows a more complete comparison of the various algorithms, since in some cases the SNR performance is most critical; in other cases, the suppression of sampling error is most critical; and in yet other cases, relative immunity to blur spot distortion (over fields of view or with optical distortion) may be most critical. We have included all those considerations in this work.

Problem definition

All the track algorithms considered estimate the position either of the peak or of the centroid of the image of a point source. The simplest means of estimating the position of the peak of the blur spot is to use a detector array and assume that the target is at the center of the detector element with the largest signal. This coarse form of position determination, however, is never more accurate than approximately one-third the detector-to-detector spacing, irrespective of the signal-to-noise ratio. This accuracy can be increased significantly by use of an interpolation procedure in conjunction with the indicated coarse search procedure. Appropriate interpolation procedures are the subject of this investigation.

The baseline point-spread function or optics blur spot was assumed to be a symmetric Gaussian with the half-width ρ. The Gaussian point-spread function is described by

$$I(x,y) = \frac{W_o}{2\pi\rho^2}\left[-(x^2+y^2)/2\rho^2\right], \tag{1}$$

where $I(x,y)$ is the intensity at (x,y) of a target blur spot centered at the origin, and W_o is the total power in the blur spot. All sizes and spacings are in arbitrary units which will be normalized to the detector size. If diffraction-limited, the Airy spot is related to the Gaussian representation by $2\sqrt{2}\rho = 1.2\lambda/d$. λ is the average spectral wavelength of interest, and d is the diameter of the optical aperture. The Gaussian blur spot is more tractable mathematically than the Airy spot, and is also an excellent approximation to its central portion, which is the region of interest. Furthermore, any smearing of the blur spot from optical aberrations or a wide spectral band will make the resultant blur spot shape tend toward a Gaussian.

The focal plane design assumed in this analysis is a close-packed mosaic array of visible detectors, such as a backside-illuminated (100% coverage) CCD mosaic. The sensor operates in the staring mode (staring at the star scene). The blur spot (point spread function) diameter is two to six detector lengths (L). Each detector is assumed to have a flat responsivity within the detector outline and none outside.

The photon flux at the detector is that due to the flux from the point source blur spot. Because we are considering star sensor design, any background is considered negligible. The detectors are integrating-type detectors, such as those fabricated in CCD's. For best analytic comparison, the detectors were assumed device-noise (CCD-noise) limited with an equal noise level for all elements. Signal shot-noise limited performance was also considered (as shown in the results) but was found to not significantly change the conclusions of the design.

The detector with the maximum signal $S_{o,o}$ defines the "coarse track" position and establishes the origin for the interpolation. The signal output $S_{n,m}$ of an individual detector n and m spacings from the origin is the integral of the point-source blur spot centered near the origin times the detector responsivity over the area of the detectors:

$$S_{n,m} = \frac{W_o r t_{int}}{2\pi\rho^2}\iint_{-\infty}^{\infty} dxdy\, \exp\left[-\frac{(x+nL-\Delta x)^2}{2\rho^2}\right]\exp\left[-\frac{(x+nL-\Delta y)^2}{2\rho^2}\right] R_\lambda(x,y) \tag{2}$$

where t_{int} is the integration time and r is the detector responsivity. The detector responsivities are assumed repeatable with a mean value of r (per unit area) and a normalized shape of $R_\lambda(x,y)$.

Assuming a flat responsivity across the area of the detector and sharp edges makes $R_\lambda(x,y)$ equal to one inside the detector (which is a square of side L) and zero outside. The resulting signal output becomes

$$S_{n,m}(\Delta x,\Delta y,L,\rho)=\frac{W_o r}{4\rho^2}\left\{\operatorname{erf}\left[\frac{1}{\sqrt{2}\rho}\,(L(n+\tfrac{1}{2})-\Delta x)\right]-\operatorname{erf}\left[\frac{1}{\sqrt{2}\rho}\,(L(n-\tfrac{1}{2})-\Delta x)\right]\right\}$$

$$\left\{\operatorname{erf}\left[\frac{1}{\sqrt{2}\rho}\,(L(m+\tfrac{1}{2})-\Delta y)\right]-\operatorname{erf}\left[\frac{1}{\sqrt{2}\rho}\,(L(m-\tfrac{1}{2})-\Delta y)\right]\right\}=W_o r t_{int}H(n,\Delta x,L,\rho)H(m,\Delta y,L,\rho), \quad (3)$$

where erf(z) is the error function,

$$\operatorname{erf}(z)=\frac{2}{\sqrt{\pi}}\int_0^z dt\,\exp(-t^2), \quad (4)$$

and $H(n,\Delta x,L,\rho)$ is a one-dimensional filling factor accounting for the detector offset and finite size (in one dimension). The maximum possible signal obtainable is defined as $S_o(L)=S_{o,o}(0,0,L,\rho)$. In this case a function C(L), depending only on L and ρ, can be defined:

$$C(L)=H(o,o,L,\rho)=\operatorname{erf}\left(\frac{L}{2\rho\sqrt{2}}\right). \quad (5)$$

The maximum signal can be defined in terms of C(L) as

$$S_o(L)=W_o r C^2(L)t_{int}. \quad (6)$$

Only pseudo-one-dimensional or rectilinear centroids for position estimation were considered. The centroids were taken along the axis of interest with signal summing along the perpendicular axis. The two axis information is, thus, separately determined.

In these interpolation algorithms, the estimated offset from the origin is defined as Δx_e. The "true" offset is Δx. We will henceforth normalize the offsets Δx_e and resultant errors to units of detector size L. Thus, the offsets Δx_e, Δx and the errors are given as fractions of a detector size L. The interpolation algorithms considered yield estimates that can be written as ratios of sums of weighted signals from a set range of pixels:

$$\Delta x_e=\frac{\sum_{n=-N}^{+N}\sum_{m=-N}^{N} f_n S_{n,m}}{\sum_n\sum_m g_n S_{n,m}} \quad (7)$$

If the point spread function is separable as discussed above (but not necessarily circularly symmetric), the offset estimate reduces to

$$\Delta x_e=\frac{\sum_n f_n H(n,\Delta x,L,\rho)}{\sum_n g_n H(n,\Delta x,L,\rho)} \quad (8)$$

where the sum along the perpendicular axis drops out for separable point spread functions.

For the centroid, the signals are weighted by the distance from the origin by defining $f_n=n$. The signal strength is normalized out by defining $g_n=1$. Other classes of algorithms are in the process of being considered[5] which, for example, fit the data to a curve and determine the position of the peak of the curve. The simplest of these is the least-squares fit of a parabola to the data points. For the three-point, least-squares fit, f_n = and $g_n=(-2,4,-2)$.

These algorithms are to be distinguished from the thresholding and centroiding algorithms that tend to be used with resolved, non-peaked target images. For a well-defined and peaked function such as a point-spread function, the use of a technique based on a peak pixel search and a fixed N-point algorithm is preferred over a technique based on a threshold search and a centroid of all pixels above the threshold. The former technique prevents the spurious inclusion of outlying noise spikes.

The optimization of the tracking array detector size for each algorithm was based on simultaneously optimizing two competing performance factors: the individual detector SNR and the track accuracy. Maximum track accuracy is obtained when the error in the position estimate Δx is minimum. The sources of error considered were systematic algorithm error, random noise, and residual detector responsivity nonuniformities after calibration.

The systematic algorithm error or bias was calculated, and its rms value over an array pitch was used as one measure of estimation error. The random noise in the output signal was propagated by variance analysis into another component of estimation error. Finally, the residual nonuniformities in the detector responsivities after calibration were propagated by variance analysis and Monte Carlo analysis into an rms spread in the algorithm error and provided a third source of error.

The SNR error term is often considered the fundamental parameter for minimization in the optimization of an array configuration. Thus, the smallest algorithm, a (2x2 square) difference or "centroid" algorithm, is sometimes the only one considered or is considered the baseline. However, performance with respect to the other sources of error: algorithm bias error or nonuniformity error or sensitivity to blur spot distortion, must also be considered and compared. The trade must include all these errors - in which case the two-point algorithm is not necessarily the best.

Sources of error

Algorithm error

The fundamental source of inaccuracy is that of the algorithm itself (here called algorithm error, or bias). Even given very accurate data, most algorithms predict peak positions different from the actual positions. Algorithm error is systematic and predictable for a known blur spot shape. It could, therefore, theoretically be eliminated with a compensating or correction algorithm. This, however, can be done successfully only when the algorithm error is larger than the other (random) sources of error and determinable. Furthermore, the effectiveness of the correction algorithm to suppress the algorithm bias error and the algorithm sensitivity to blur spot distortion varies with the choice of algorithm (and, thus, the choise of correction algorithm). For example, if correction algorithms of comparable complexity (or look-up table size) can suppress the error by a factor of 10, then the algorithms with the smaller original error will have the smaller residual error. Furthermore, as shown in the results, the higher the spatial frequency components making up the error, the more difficult it is to correct.

The algorithm error is found by calculating the signals for a known offset Δx_e from the algorithm [Eq. (7) or (8)], and then determining the difference between Δx and Δx_e. The magnitude of this error varies with the offset Δx (Fig. 1). The symmetries of both the blur spot signal factor $H(n,\Delta x,L,p)$ and the algorithm coefficients f_n,g_n are such that Δx_e is antisymmetrical in Δx. Because of this symmetry, the mean error over the full range of offsets (from -P/2 to P/2) is zero. The rms value is, therefore, used as a measure of the error for the optimization.

Another source of algorithm error is systematic intracellular nonuniformities repeated within each detector element. Responsivity nonuniformities within the detector elements are difficult to account for analytically. But if the nonuniformity is known and repeated from cell to cell (as when the detector edges are not considered sharp, but smoothly rounded), then its effect may be incorporated into the predicted offset signal and, thus, into the offset (Δx_e). Thus, Eq. (8) is solved: but now all the S_n are the more complicated outputs of the blur spot correlated with a nonflat-response function. This, then, produces a change in the algorithm bias. This change may increase or decrease the net bias error and as defined is also systematic.

Signal-to-noise error

Another important source of error is that due to finite SNR. Noise introduces uncertainty in the data values, which propagates into an uncertainty in the knowledge of the peak position. Because SNR values in star sensor systems may be very low, this may be the dominant source of error. Variance analysis was used to determine the uncertainty in the algorithm output as a function of signal uncertainty (noise). The uncertainty in the position estimate (Δx_e) is measured by its standard deviation:

$$\sigma_{\Delta x} = \mathrm{var}^{1/2}(\Delta x_e) = \left\{ \sum_n \sum_m \left(\frac{\partial(\Delta x_e)}{\partial S_{n,m}} \right)^2 \mathrm{var} S_{n,m} \right\}^{1/2} , \tag{9}$$

where each signal is considered an independent variable, and the noise is assumed to be uncorrelated. The specific equation for the estimated position [from Eq. (7)] results in

$$\sigma_{\Delta x} = \mathrm{var}^{1/2}(\Delta x_e) = \frac{1}{\sum_n \sum_m g_n S_{n,m}} \left\{ \sum_{nm} \left(f_n - g_n \Delta x_e \right)^2 \mathrm{var} S_{n,m} \right\}^{1/2} , \tag{10}$$

where f_n,g_n are the algorithm coefficients.

The factor $\mathrm{var}S_{n,m}$ in Eqs. (9) and (10) is the square of the detector noise N_{CCD}. It is the same for all detectors and can, therefore, be factored out of the sum of the equations. The maximum signal $S_o(L)$ can be incorporated into the denominator, resulting in

$$\sigma_{\Delta x} = \mathrm{var}^{\frac{1}{2}}(\Delta x_e) = \left(\frac{N_{CCD}}{S_o(L)}\right) \frac{C^2(L)/H(o,\Delta y,L,o)}{\sum\sum_{n\,m} g_n H(n,\Delta x,L,o)} \times \left\{\sum\sum_{n\,m} (f_n - g_n\,\Delta x_e)^2\right\}^{\frac{1}{2}} \tag{11}$$

It is obvious that the noise error [Eq. (11)] contains the inverse of a signal-to-noise ratio. We could simply define the signal-to-noise ratio as the ratio of the maximum possible signal on a single detector, $S_o(L)$, to the single detector device (or CCD) noise level N_{CCD}. The noise level N_{CCD} is assumed the same for all detectors. The resulting signal-to-noise ratio would be

$$SNR = \frac{S_o(L)}{N_{CCD}} \tag{12}$$

This is not the actual SNR occurring at any detector but is the maximum possible SNR which would result if the blur spot were centered on that detector.

However, one of the goals of this analysis is to determine the detector size that minimizes the noise-induced error in the peak position estimate. One cannot just minimize the factors multiplying the inverse signal-to-noise ratio described in Eq. (11) because there is still a size dependence in the signal-to-noise ratio. In order to optimize the size and spacing of the detectors, this dependence must be explicit. The area dependence of $S_o(L)$ has already been given in Eq. (3). The CCD noise is independent of the detector area. Thus, one can easily define a new SNR factor consisting of the effective "total signal" due to the total blur spot divided by the noise on one detector. This eliminates the dependence on the detector count in the algorithm and allows a valid comparison for centroids of different detector counts.

$$SNR_o = \frac{W_o r t_{int}}{N_{CCD}} = \frac{SNR}{C^2(L)} \tag{13}$$

The resulting SNR error becomes

$$\sigma_{\Delta x} = \mathrm{var}^{\frac{1}{2}}(\Delta x_e) = \frac{1}{SNR_o} \frac{1}{\sum\sum_{n\,m} g_n H(n,\Delta x,L,o) H(m,\Delta y,L,o)} \left\{\sum_n \sum_m [f_n - g_n\,\Delta x_e]^2\right\}^{\frac{1}{2}} \tag{14}$$

Both Eqs. (11) and (14) clearly show that the error in the peak position estimate varies as SNR^{-1}.

A different noise source would have required a different analysis.[5] For instance, including a signal shot-noise would have required an additional noise source

$$N \rightarrow \left(N_{CCD}^2 + S_{n,m}\right)^{\frac{1}{2}} = N_{CCD}\left(1 + \frac{SNR_o}{N_{CCD}} H(n,\Delta x,L,o) H(m,\Delta y,L,o)\right)^{\frac{1}{2}} \tag{15}$$

where now we must be explicit that both the signal, $S_{n,m}$, and the noise, N_{CCD}, are in units of charge. The equivalent signal shot-noise is represented by

$$N_{n,m} = [N_{CCD} SNR_o H(n,\Delta x,L) H(m,\Delta y,L)]^{\frac{1}{2}} \tag{16}$$

Nonuniformity error

Variation in responsivity from detector to detector is a third important source of uncertainty. Much of the detector-to-detector response variation in mean responsivity can be removed with a gain and offset calibration. The residual nonuniformity, typically ½ to several percent, acts as a limit to the accuracy of the data points and, therefore, of the predicted position. The uncertainty due to residual responsivity nonuniformity can be calculated from a derivation that is similar to that for the SNR uncertainty, provided that the residue is assumed random.

The residual uncertainty in the responsivity can be represented as a fractional uncertainty in r:

$$\delta = \frac{\sigma(r)}{r} = \frac{\mathrm{var}^{\frac{1}{2}} r}{r} . \tag{17}$$

The variance of the signal [from Eq. (3)] becomes

$$\mathrm{var}S_{n,m} = S_{n,m} \frac{\mathrm{var}\, r}{r^2} = S_{n,m}^2 \delta^2 . \tag{18}$$

on into the variance of the position estimate [Eq. (10)] results in

$$= \frac{\delta}{\sum_n \sum_m g_n H(n,\Delta x,L,\rho)H(m,\Delta y,L,\rho)} \times \left\{ \sum_n \sum_m (f_n - g_n \Delta x_e)^2 H^2(n,\Delta x,L,\rho)H^2(m,\Delta y,L,\rho) \right\}^{\frac{1}{2}} \quad (19)$$

ility is again assumed [Eq. (4)].

Total effect of error sources on algorithm accuracy

the errors, the total uncertainty in the prediction of the peak signal posi-
direction) is

$$\sigma_{\Delta x_e}(\Delta x) = \left(B^2(L,\rho,\Delta x) + \frac{A^2(L,\rho,\Delta x)}{SNR_0^2} + D^2(L,\rho,\Delta x)\delta^2 \right)^{\frac{1}{2}} , \quad (20)$$

e error at Δx due to algorithm bias or inherent algorithm inaccuracy, A is a
factor at Δx (containing all the detector size dependence) for the signal-to-
and D is a configuration factor at Δx for the error due to the residual
(after calibration) in the mean responsivity from detector to detector.

cking loop is closed around the sensor, holding the blur spot to the center of
great accuracy, then the error is essentially that occurring around $\Delta x = 0$:

$$\Delta x_e = \left(\frac{A^2(L,\rho,0)}{SNR_0^2} + D^2(L,\rho,0)\delta^2 \right)^{\frac{1}{2}} \quad (21)$$

orithm bias goes to zero at the origin by symmetry. This equation should
lone to optimize the configuration design. The slope of the algorithm
, at $\Delta x = 0$ can be considered the ratio of the error in the estimated position
in the actual position at the null point and, thus, must also be included.
the error in the estimated position $\sigma_{\Delta x}$ to the error in the actual position
oint and, thus, must also be included. The ratio

$$= \sigma_{\Delta x}(0) \Big/ \left. \frac{dB(L,\rho,\Delta x)}{d\Delta x} \right|_{\Delta x = 0} \quad (22)$$

ized for the smallest uncertainty about $\Delta x = 0$. Our analysis did not,
sue the closed-loop behavior because that is only appropriate for a null
as a quad cell) and was not considered to fulfill the needs of the SIRTF

he sensor was considered to run open loop. The sensor estimated the position
urce without tracking it, giving the image an equal probability of falling
in a pitch. The error averaged over a whole interval should then be used
of expected performance. In that case, the mean of A and D and the standard
B (whose mean is 0 by symmetry) can be used.

$$\left(\frac{A^2}{SNR^2} + \bar{D}^2\delta^2 \right)^{1/2} \quad (23)$$

is indicates that the sensor accuracy versus SNR should show two asymptotic
vior. The SNR error dominates for low SNR values with a SNR^{-1} dependence
ficiently high values, it falls below the level of the algorithm bias error.
rection algorithm is used to suppress the systematic algorithm error, the
ultimately be limited by the residual algorithm bias error or a constant
or calibration error.

Parametric analysis of performance behavior

s error sources are evaluated separately. The configuration evaluated
packed case where the detector center-to-center spacing is also the detector
star sensors or tracking sensors a certain field-of-view (FOV) must be
m available CCD configurations, or focal plane design limitations, this
nt places a footprint size requirement on the detector element. Thus the
print or effective size, L, is constrained. However, if the detector sizes
an the diffraction-limited point spread function, the blur spot size can
larged) to obtain the best match for performance.

zation of the SNR error is of special importance when dealing with sensors,
sensors and imaging sensors, observing "external" sources. Sensors with
urces such as those in alignment or wavefront sensing systems have more
the signal strength (SNR factor) and are, thus, optimized almost solely
to the other sources of error (primarily the algorithm bias error). Further-

more, these alignment or tracking sensors may be in systems where the blur spot size is predetermined (for instance, diffraction-limited) and there is relatively small FOV coverage. For the optimization of these sensors, therefore, the following analysis would be more useful if the results were presented in units of blur spot diameter rather than the "inverse" units of detector size.[5]

SNR error performance

Taking the SNR performance into initial consideration, Fig. 2 shows the averaged SNR factor $\bar{A}$ [Eq. (23)] for several different algorithms as a function of blur spot size relative to the detector size (where the blur spot size is considered $4\sqrt{2}\sigma$ from Eq. (1)). The performance factor $\bar{A}$ is in units of detector size L. The general behavior for all algorithms is an improvement in performance as the blur spot decreases in size until a saturation occurs at about the point that the algorithm gate (NxN detectors) just covers the blur spot. Decreasing the size further results in no further improvement relative to the SNR performance. Thus, the SNR behavior is one factor in limiting the size of the blur spot.

The SNR behavior (A) can be asymptotically approximated for large blur spot sizes by noting that all the signals in the denominator in Eq. (14) can be approximated by the sum of an exponential times the detector size (Eq. (2) or (3) for small L)

$$A = \sigma_{\Delta x}\,\mathrm{SNR}_o = \frac{\left[\sum\sum (f_n - g_n\,\Delta x_e)^2\right]^{1/2}}{\sum\sum_{hm} g_n\, S_o\,(L)} \approx \frac{2\pi\sigma_o^2/L^2}{N^2 W_o r t_{int}} \left\{\sum\sum (f_n - g_n\,\Delta x_e)^4\right\}^{1/2} \qquad (24)$$

where A (or $\sigma_{\Delta x}$) is normalized to units of detector length. N is the number of points in an NxN centroid and $g_n \approx 1$. The result implies that the SNR error factor quickly goes up as the area of the blur spot.

The saturation behavior at the lower blur spot sizes shows an expected improvement in performance as the detector count decreases (fewer sources of CCD noise). This asymptotic behavior can be evaluated explicitly for small blur spot sizes by letting the sum in the denominator in Eq. (14) go to unity (complete coverage of the blur spot by the algorithm gate) and summing the f_n and g_n in the numerator with an assumed value for Δx_e^2 of ~ 1/12. These correspond to the limits in the figure.

Thus, with respect to signal-to-noise performance, the often used (2x2) point algorithm is the best - with a 40% improvement over the next best (3x3) point algorithm. However, we will show that for many sensor designs that factor of 2 may not be the deciding factor in the choice of algorithms.

Algorithm Bias Error Performance

These star sensors and other point source sensors are required to determine the geometric position of a point source to some accuracy over the whole field-of-view. Thus, even if the jitter (SNR error) is reduced sufficiently, there is still a positional or bias requirement. This is precisely the algorithm bias error discussed earlier. Fig. 3 shows the (rms) averaged algorithm bias error $\bar{B}$ (from Eq. (23)) in units of detector size L, as a function of blur spot size (which is also in units of detector size). Almost the inverse behavior occurs. The fewer points in the algorithm, the larger the minimum in algorithm error and the narrower the operating range. This occurs because the larger count centroids do a better simulation of a continuous centroid. The convergence of all the algorithms for small blur spot sizes occurs because only the difference between the innermost pair of detectors is of significance irrespective of how many detectors are used in the algorithm.

For all the algorithms, the region of minimal error tends to occur in the saturation region of SNR performance (compare Fig. 3 to Fig. 2). Thus, design of the sensor to minimize algorithm bias error ($\bar{B}$) for a particular algorithm will automatically obtain optimum SNR performance. However, this optimum blur spot size is different for different algorithms - thus, making the choice of algorithm of critical importance. The (2x2) point algorithm has the best SNR performance - but at the cost of the worst algorithm bias error. The 3 point algorithm has a factor of 2 worse SNR performance but has significantly better algorithm bias error performance. If extreme positional accuracy is required, this better performance may be critical.

Algorithm bias error is a fixed, systematic error that can be suppressed by calibration procedures. However, as we will show, this reduction of the error is not perfect, has glaring limitations and, effectively, only tends to reduce the scale in Fig. 3, not changing the order of the performance. The (3x3) point algorithm remains significantly better than the (2x2) point algorithm from the standpoint of algorithm bias error.

A computer evaluation of the prediction of the offset by several interpolation procedures for a typical case was shown in Fig. 1. The algorithms are not perfect in their prediciton but may have errors that can be corrected with a minimum of effort such as a small look-up table, or preferably, with simple correction functions such as a linear scale factor

$$\Delta x_e' = (1+s)\Delta x_e \tag{25}$$

or a sinusoidal correction

$$\Delta x_e' = \Delta x_e + s\sin(\pi\Delta x_e) \tag{26}$$

The simple linear scale factor is, of course, the easiest correction to make.

The major issue then becomes: what is the sensitivity of this correction algorithm (or look-up table) to changes in blur spot size or blur spot shape? These changes can easily occur as the optics distorts due to thermal gradients or - much more significantly - as the spot varies across the field-of-view (FOV) of the sensor. If there is a great sensitivity to the blur spot distortion, then the calibration becomes unwieldy (many field points must be evaluated in detail), the computational requirements go up significantly and quickly (a very large look-up table becomes required) and the stability requirement becomes extreme.

Figs. 4, 5, and 7 show the significance of this concern. They show the algorithm bias error at the optimum blur spot size as a function of offset for circular spots and spots with only ±20% distortion along one axis (R = 0.8 or 1.2).

Fig. 4 is for the (2x2) algorithm and shows a very distorted error with extreme errors much larger than the average. Linear and sine corrections did not succeed in reducing the error. Only a direct look-up table for the undistorted spot was at all useful. However, a 20% distortion was sufficient to nullify the effect of the look-up table resulting in errors nearly as large as without correction. Thus, the (2x2) point algorithm is very sensitive to blur spot distortion which could present difficulties in sensor design with significant FOV's.

Fig. 5 is for the (3x3) algorithm and shows a moderate error that is nearly linear. Fig. 6 shows that the blur spot size of minimum error (diameter = 2.3L) is also the cross-over point between a simple linear error (for larger blur spot sizes) and a simple sinusoidal-like error (for smaller blur spot sizes). Thus, this error is easily functionally correctable and even if the blur spot size were not optimum, the correction could still be a simple linear scale factor or a simple sine term. Furthermore, if the spot distorts by elongation, the simple linear correction is more effective over a larger distortion range. Furthermore, if the distortion can be estimated - such as a coma - the linear scale factor can be treated in a simple manner as a function dependent on FOV position - increasinng its effectiveness.

Fig. 7 shows the even better performance occurring with a (4x4) point algorithm. The penalty is in the significantly higher SNR factor (Fig. 2).

These performance ranges for the various algorithms are quantified in Fig. 8. The rms-averaged uncorrected algorithm bias errors as a function fo blur spot distortion are shown as the solid lines. The algorithm bias error after application of the above mentioned correction procedures are shown in the dashed lines. Note, however, that we are as yet only considering elongation along one axis only. Radial elongation in the FOV has not yet been considered in this analysis but will be incorporated in the future.

Uncorrected, the (2x2) algorithm error is significantly worse than the (3x3) point. Even with correction, the range of effectiveness of the correction is much narrower than for the (3x3) point. If there is signal power to spare, then the (5x5) point algorithm is very insensitive to distortion and would be the preferred algorithm.

This chart also indicates the expected limiting algorithm bias performance of the various algorithm candidates. Assuming very good optics and a narrow enough FOV resulting in only ±10% blur spot variation over the FOV, a (2x2) algorithm will perform to a level of ~ 1/30 a detector (or ~ 1/100 a blur spot) accuracy without correction. With a look-up table correction, the limiting accuracy may become ~ 1/50 detector. The (3x3) algorithm will have a limiting performance of ~ 1/75 a detector (or ~ 1/200 a blur spot) uncorrected. With correction, the limiting performance will be ~ 1/200 a detector. The (4x4) and (5x5) algorithms will be better than 1/300 a detector (or 1/600 a blur spot).

However, if the FOV is large enough that the blur spot may have significant variation, the (2x2) algorithm degrades much quicker than the (3x3) algorithm. For example, if a coma-like distortion of 50% is allowed, the average performance of the (2x2) algorithm is ~ 1/15 a detector uncorrected and ~ 1/22 a detector corrected. The (3x3) point algorithm, on the other hand, has a limiting accuracy of ~ 1/37 detector uncorrected (> 2 times as good) and ~ 1/60 detector corrected (~ 3 times as good). If there is sufficient signal, the (5x5) algorithm still has > 1/300 detector accuracy while uncorrected.

Thus, the poorer algorithm bias performance of the (2x2) algorithm may limit its usefulness in the design of point-source tracking sensors. If the texternal sources are weak (high magnitude stars, for example) and the positional accuracy requirement is not too great, then the SNR performance takes precedence and a (2x2) algorithm should be used. If the positional accuracy requirement is sufficiently stringent and/or the blur spot distortion is not insignificant, then a (3x3) algorithm should be used (the SNR performance, may have to be regained by a larger optics aperture). If the positional accuracy requirement is extreme, then a (4x4) or even a (5x5) algorithm will have to be used. These results will be applied towards the SIRTF star sensor in the next section.

Nonuniformity error performance

The rms responsivity nonuniformity error factor for the various algorithms as a function of blur spot size is shown in Fig. 9. Comparing the nonuniformity factor to the algorithm error indicates the levels at which the nonuniformity degradation begins to dominate. If the algorithm bias, especially with a good correction algorithm, is sufficiently small, then the nonuniformity error will be the residual system error. Even this error can be reduced with responsivity calibration. Its level, therefore, has impact on whether a point-by-point detector calibration is required, and if it is, then to what level of accuracy. Only the high spatial frequency component of the nonuniformity is relevant (the nonuniformity within a range of N detectors for a NxN algorithm) and is typically 1% - 4% for visible CCD's.

Fig. 9 indicates that for visible CCD's of typical 1% to 4% local nonuniformities, the nonuniformity errors will not be of significance (even with algorithm bias correction) for the (2x2) or (3x3) algorithms. Thus, detailed point-by-point responsivity calibration will only be required for extreme pointing requirements which also require (4x4) or (5x5) algorithms. This does not apply to point-by-point electronics offset subtraction (fixed pattern suppression), or to mosaics with larger nonuniformities (such as IRCCD's).

Monte Carlo results

A Monte Carlo simulation of the peak location algorithms in the cross-scan direction was performed to determine the limits of the validity of the variance analysis and to more completely evaluate the effects of the coarse search procedure and the responsivity nonuniformity. The data to be fitted were one set of detector outputs where the blur spot was assumed centered on the array. The blur spot was assumed Gaussian and offset Δx from the center of the central detector. The Monte Carlo program generated statistical ensembles of focal planes with varying amounts of responsivity nonuniformity. Six focal planes were generated for each of five levels of rms nonuniformity ranging from 0 to 4%. The program then generated a separate statistical ensemble of 200 signals at each of 15 signal-to-noise ratios for each focal plane. A simple search for the peak signal was normally used as the coarse search procedure. However, in some Monte Carlo tests, the origin was a priori taken at the center detector in order to separate out the effects of the coarse track procedure. The estimated offset Δx_e from the center detector was calculated for each sample of the ensemble by the interpolation procedure. The statistical variance of $(\Delta x_e - x)$ was then calculated. This error was compared to the error predicted by the variance analysis for the SNR uncertainty and the algorithm bias by determining the asymptotic 1/SNR behavior for small SNR and the asymptotic constant level for large SNR due to the algorithm bias (here treated as a noise).

Figure 10 shows Monte Carlo results taken assuming uniform detector responsivities. The results confirm the SNR factor and algorithm bias error magnitudes obtained from the variance analysis for all but the smallest signal-to-noise ratios. For SNR values ≤ 6, the Monte Carlo results diverge from the analytic behavior. Part of the reason for the divergence is the poor performance of the coarse search procedure at low SNR, but part is because of the failure of the statistical assumptions implied by the variance analysis. Because there is a slight offset dependence on $A(\Delta x)$ (Fig. 11), the analytical result was taken from the $\Delta x = 0$ and $\Delta x = .25$ cases, not the averaged value shown in Fig. 2.

Fig. 12 compares the analytic and Monte Carlo behavior with the inclusion of signal shot noise. A low CCD noise level of 40e is assumed. There is no significant difference at the critical moderate SNR values where the performance is marginal. Even at the higher

SNR values, the degradation in performance is still moderate and still allows the performance to more than meet the requirement.

As noted, the Monte Carlo program was also run for various levels of array nonuniformity. The ensemble spread of algorithm biases (versus nonuniformity) was compared to the predicted rms spread (at the given offset) for the (3x3) algorithm. The Monte Carlo results are compatible with the statistical definition of the calculated spread (fig. 12).

Application to the SIRTF fine guidance sensor

The system requirements are listed in Table I. The basic pointing requirements (listed as Top Level) were reduced to a generic design (listed as Baseline Design) in previous SIRTF studies.[6] This choice of FOV diameter and star magnitude sensitivity is, however, really not fixed but is parametrically related. The FOV requirement to see two stars can be derived from the stellar densities[7] and plotted versus their stellar magnitudes (Fig. 14). Over a sufficiently large range we may consider the FOV diameter requirement to go exponentially as the stellar magnitude (from Fig. 14, down to 10th magnitude). Given a choice only of commercially designed CCD chips and assuming a single CCD chip focal plane, the angular footprint of one detector element is predetermined

$$L = \frac{FOV}{n_{CCD}} \tag{27}$$

where FOV is the angular FOV requirement and n_{CCD} is the number of detector elements along one axis. The system positional accuracy requirement can be transformed into units of a fraction of a detector. This is done in the vertical scales to the right of Fig. 14.

Using Fig. 8 as a measure of average algorithm bias error - which translates directly into positional error - we can determine if there are any limits on the range of FOV/star magnitude in the design. If the optics were perfect and without distortion and a TV-type (RCA) CCD chip were used (as in the baseline[6]), the (2x2) algorithm would still be limited to FOV's smaller than 0.4 degree diameter. The sensor would, thus, have to be sensitive enough to track stars of magnitude greater than 12 to the accuracy required. With the same perfect optics and RCA CCD, the (3x3) algorithm would allow a choice of FOV from the whole range - up to 1.0 degree diameter.

However, the SIRTF optics will not be perfect in the visible, and 30% elongation may well occur at the edges of the FOV or due to thermal gradients. If this occurs, the (2x2) algorithm (from Fig. 8) now limits the design to a FOV diameter < 2.5 degree in order to meet the requirement at the edges of the FOV. The (3x3) algorithm still leaves a choice of most of the range (FOV diameter < 0.7 degree).

Thus, for an RCA chip and (2x2) algorithm, the choice of the smallest FOV of the range (~ 0.2 degree dimaeter) and tracking capability of 14th magnitude stars is essentially forced upon the design. However, we will consider (3x3) algorithms and even the impact of using a Galileo-type (800 x 800) TI CCD chip.

For the (3x3) algorithm with the RCA chip, and for both algorithms with the TI chip, a range of FOV diameters - and, thus, limiting star magnitudes for tracking - is available. Our derivation of the SNR performance obtained a result ($\bar{A}$) in units of detector element size L

$$\sigma_{SNR} = \frac{\bar{A}\, L}{SNR} \tag{28}$$

where now the units are, for example, angular. The signal can be normalized to the signal from a 14th magnitude star by

$$SNR_m = (2.51)^{14-m}\, SNR_{14}. \tag{29}$$

Over several stellar magnitudes the FOV requirement can be related to the magnitude by

$$FOV = FOV_{14}\, 10^{(14-m)/5} \tag{30}$$

Substitution of these two equations and Eq. (27) into Eq. (28) results in

$$\sigma_{SNR} = \frac{\bar{A}}{n_{CCD}} \frac{FOV_{14}}{SNR_{14}} (0.63)^{14-m} \tag{31}$$

Thus, the larger the FOV becomes (within the allowed range discussed above) - with a corresponding decrease in the required magnitude of the guide stars - the better the performance becomes. For the design of a (2x2) algorithm with a RCA chip, there is

no range due to the large algorithm bias error. The baseline design of ~ 0.25 degree diameter FOV with sufficient sensitivity to track 14th magnitude stars then remains the best choice. However, the use of a (3x3) algorithm allows a larger FOV design with a corresponding lower sensitivity requirement for lower magnitude stars (limited by its algorithm bias error). With a (3x3) algorithm design, a FOV ~ 0.7 degree diameter (assuming no greater optical degradation at this larger FOV) and use of m=11 guide stars results in the optimum design. The SNR error with this design and the (3x3) algorithm is 0.25 the error with the baseline design and the (3x3) algorithm and even 0.5 the error of the (2x2) algorithm with the baseline design. This occurs because the m=11 stars are so much brighter.

As indicated by this analysis the final design configuration of the fine guidance sensor is highly dependent ont he performance of the optics, and a final design would have to await detailed optical design with output of blur spot distortion over the FOV and thermal gradient effects. The choice of FOV and even of the algorithm are very sensitive to the quality of the optics. With perfect, undistorted optics, the greater SNR performance of the (2x2) algorithm would make it the theoretical favorite. However, with realistic optical performance, the much greater sensitivity of the (2x2) algorithm to optical distortion makes the (3x3) algorithm the realistic favorite candidate.

Design of the SIRTF FGS sensor

Both the baseline design (in Table I) and the optimized variants will be considered. Both designs will assume optics that have blur spot deformations (such as elongation) less than 30% over the whole FOV. Finally, the improvement available with a TI (800 x 800) CCD chip will also be evaluated. The master relation for evaluation fo the signal to noise is

$$SNR_o = \frac{\text{"SIGNAL" FROM BLUR SPOT}}{\text{CCD NOISE ON 1 DET}} = \frac{\text{RESPONSIVITY} \times P_{BLUR} \times \tau}{N_{CCD}}$$

$$= \frac{\eta_o A_o \tau G}{N_{CCD}} \int d\lambda \eta(\lambda) P_T(\lambda) = \frac{\eta_o A_o \tau G}{N_{CCD}} \overline{\eta P_T \Delta\lambda} \; (2.51)^{-(m+26.9)} \qquad (32)$$

where η_o is the optics transmission (including occultation), A_o is the total aperture area, τ is the integration time, G is the detector gain, N_{CCD} is the detector CCD noise, $\eta(\lambda)$ is the detector quantum efficiency at the wavelength λ (or the flux of a 5900°K blackbody which is considered the source) and m is the stellar magnitude of the guide star (scaling down its incident flux). Most of this was taken with verification from the previous JPL report.[6]

For an internal fine guidance sensor the optical aperture diameter is the SIRTF telescope aperture used in a shared mode (70 cm diameter). A moderate visible transmission (including occultation) of 36% is expected. The update rate requirement with a chopping mode of operation limiting the integration time results in a τ =0.45 sec.

Table II shows the performance of various candidate designs. The N/A means that irrespective of SNR performance, the FOV is too small to insure seeing 2 guide stars in that FOV. First is the expected performance of the baseline established on previous studies with the (2x2) algorithm (1). It does not meet the positional accuracy requirement because of the algorithm bias error - as discussed before, it is very sensitive to blur spot distortion. Though it only marginally misses the requirement, the other alternatives are more attractive. Using the same baseline but a (3x3) algorithm (3) results in sufficient performance to meet the positional requirements, but the performance is too marginal for the jitter error (or SNR error).

Changing only the FOV (5) and using the (3x3) algorithm allows a significant improvement with about a factor of 3 margin in the signal collection efficiency (algorithm bias error limited rather than SNR limited) and allows operation with 12th magnitude (and even 13th magnitude) stars.

The use of the large TI CCD (800 x 800) allows satisfactory performance with either of the algorithms [(2) and (4)]. In essence, the detector footprint is now sufficiently small with the 900 arcsec FOV to generate a weak enough position requirement ($\sigma \leq L/8$) to make the algorithm bias error a negligible issue. One can take advantage of the large detector count on the chip by opening up the FOV to accommodate 11th magnitude stars (6). Using a (3x3) algorithm, the algorithm bias error is still held to 0.05 arcsec, well within spec, and the sensitivity is sufficient to meet the jitter requirement with a factor of 100 margin for 11th magnitude stars. It can even meet the requirements using up to 14th magnitude stars.

Finally, if the FGS is designed to be boresighted using a separate telescope, the telescope can be made much smaller [as seen in (7) and (8)] and the visible optical

quality can be held under much better control and chopping techniques are not a concern.

Conclusion

In the design of the SIRTF Fine Guidance Sensor (FGS), the general issues of design optimization fo a staring mosaic sensor for guide-star tracking and the choice of the proper interpolation algorithm were considered. The (2x2), (3x3), (4x4) and (5x5) centroid interpolation algorithms were evaluated. Though the sensor was considered a staring sensor, it was not considered a nulling sensor; the guide stars would be imaged any place within the field-of-view (FOV) and any place on the detector elements. The performance was, thus, averaged over all possible offsets from the center of a detector.

The blur spots were gaussian or elongated gaussian and the detectors had unity responsivity within their footprint and zero responsivity outside (and sharp transitions). Because of fixed FOV requirements and limited choices of CCD's, the detector footprints were of fixed size and all performance parameters were evaluated in units of detector size L.

The jitter error (SNR error) decreased until it saturated at blur spot ($4\sqrt{2}\sigma$) sizes which just covered the number of detectors in the algorithm (NxN). The smaller the number of points in the algorithm, the lower the residual SNR error. The (2x2) algorithm has the lowest error with about a factor of 2 better performance than the (3x3) algorithm.

The positional error or algorithm bias error has the inverse dependence with a lower minimum error as the algorithm detector count increases. Thus, the (2x2) algorithm has more than 2 times greater a minimum positional error than the (3x3) algorithm.

The algorithm bias error can be theoretically suppressed with a correction algorithm or a look-up table. However, the sensitivity of this correction technique to blur spot distortion or mismatch increases significantly as the detector count decreases. Thus, for a (2x2) algorithm, a 10-15% distortion of the blur spot nullifies the correction procedure. A (3x3) algorithm is less sensitive, allowing blur spot distortion out to 30-50%.

The final choice of algorithm depends on the severity of the positional accuracy requirement and the expected variation in the blur spot shape. The limited positional accuracy of the (2x2) algorithm and the extreme sensitivity of its correction techniques to blur spot distortion make the (3x3) algorithm often the one of choice. Only when the positional accuracy requirement is very weak ($\geq$ L/20) might one consider the (2x2) algorithm.

The SIRTF Fine Guidance Sensor (FGS) was optimized using the results of this analysis. The baseline design marginally did not meet the performance requirements. The design was optimized with lower magnitude guide stars (12th to 13th) and a larger FOV (to insure seeing the required two stars for guidance) to enable all the pointing requirements to be met. A FOV = 1600 arcsec diameter, allowing 12th magnitude stars to be guide stars, and a (3x3) algorithm is an optimized design resulting in ~ 0.08 arcsec positional error and ~ 0.03 arcsec jitter error. If a TI CCD (800 x 800) is used instead of the baseline RCA chip, the performance requirements are easily met with almost any configuration. The most margin occurs, however, with a design using a FOV = 2300 arcsec, allowing the use of stars down to 11th magnitude as guide stars, and a (3x3) algorithm, resulting in a positional error of 0.05 arcsec and a jitter error of < 0.03 arcsec for stars of 11th to 13th magnitude (and even 0.06 arcsec error for stars of 14th magnitude). From the design point-of-view an external FGS offers improved performance with much smaller aperture optics (~ 25 cm diameter) which, because they are dedicated optics, will have better figures of merit and do not share any of the problems of the internal guidance sensor.

Acknowledgements

Some of this work was done under NASA Ames Contract NAS-2-11550. I wish also to acknowledge the fruitful discussions with R. B. Emmons and the heroic typing effort by Mary Haro.

References

1. J. Allen Cox, in Processing of Images and Data from Optical Sensors, W. H. Carter, ed., Proc. SPIE 292, 288 (1981).
2. L. Cassidy and L. Kaplan, in Shuttle Pointing of Electro-Optical Experiments, W. Jerkovsky, ed., Proc. SPIE 265, 219 (1981).
3. E. W. Dennison and R. H. Stanton, in Smart Sensors II, D. F. Barbe, ed., Proc. SPIE 252, 54 (1980).
4. P. M. Salomon and T. A. Glavich, in Smart Sensors II, D. F. Barbe, ed., Proc. SPIE 252, 64 (1980).

5. S. B. Grossman and R. B. Emmons, in Optical Engineering 23, 167 (March/April 1984).
6. SIRTF Fine Guidance Sensor Imager Study, Tech. Rpt., Jet Propulsion Labs, (1982).
7. Astrophysical Quantities, C. W. Allen.

Table 1 SUGGESTED SIRTF FGS REQUIREMENTS AND BASELINE DESIGN

TOP LEVEL:

- ≤ 0.15-arcsec POSITIONAL (BIAS) ERROR
- ≤ 0.1-arcsec rms ERROR
- HAVE SUFFICIENT FOV AND SENSITIVITY TO ALWAYS BE ABLE TO TRACK ON TWO STARS IN THE FOV
- ≤ 1-s DATA RATE

BASELINE DESIGN:

- FOV DIA = 900 arcsec (15 arcmin)
- SENSITIVITY SUFFICIENT TO TRACK ON 14th MAGNITUDE STARS (MINIMUM MAGNITUDE STARS WITH DENSITY SUFFICIENT TO INSURE ≥2-in. FOV)
- 1 RCA CHIP (320 x 512, BUT EFFECTIVELY 320 x 320)
  - rms ERROR = $\frac{L_{DET}}{28}$
  - bias ERROR = $\frac{L_{DET}}{19}$
- BLUR SPOT WIDTH ≅ TWO DETECTORS
  - MAY BE LARGER THAN THE DIFFRACTION LIMIT

Table 2 FGS DESIGN ALTERNATIVES

		BASELINE (2 x 2)		BASELINE (3 x 3)		NEW FOVs		EXTERNAL TELESCOPE	
CCD CHIP		RCA[1]	TI[2]	RCA[1]	TI[2]	RCA[1]	TI[2]	RCA	TI
APERTURE DIAMETER	(cm)	70	70	70	70	70	70	52.5	25
FOV DIAMETER	(arcsec)	900	900	900	900	1600	2300	1600	2300
L_{DET}	(arcsec)	2.8	1.13	2.8	1.13	5.0	2.9	5.0	2.9
ALGORITHM		(2 x 2)	(2 x 2)	(3 x 3)	(3 x 3)	(3 x 3)	(3 x 3)	(3 x 3)	(3 x 3)
ALG BIAS ERROR* $_{BIAS} = \bar{B}$	(arcsec)	0.16	0.06	0.05	0.02	0.08	0.05	0.08	0.05
SNR ERROR σ_{SNR} (14th MAGN.)	(arcsec)	0.05	0.01	0.09	0.02	0.16	0.06	0.13	0.20
σ_{SNR} (13th)	(arcsec)	N/A	N/A	N/A	N/A	0.07	0.02	0.05	0.08
σ_{SNR} (12th)	(arcsec)	N/A	N/A	N/A	N/A	0.03	0.01	0.02	0.03
σ_{SNR} (11th)	(arcsec)	N/A	N/A	N/A	N/A	N/A	<0.01	N/A	<0.01

1 ASSUME: 320 PIXELS/AXIS; 80 (e) NOISE LEVEL; $\overline{\eta P_{T\Delta\lambda}} = 1.9 \times 10^{17}$ (e/cm^2-s); $\tau_{int} = 0.45$ s; $\eta_{OPT} = 0.36$

2 ASSUME: 800 PIXELS/AXIS; 30 (e) NOISE LEVEL; $\overline{\eta P_{T\Delta\lambda}} = 1.2 \times 10^{17}$ (e/cm^2-s); $\tau_{int} = 0.45$ s; $\eta_{OPT} = 0.36$

* A 30% BLUR SPOT VARIATION IS ASSUMED AND THE WORSE CASE PERFORMANCE (AT EDGES) IS SHOWN

N/A = MEANS FOV IS NOT SUFFICIENT TO INSURE; THERE WILL BE TWO GUIDE START

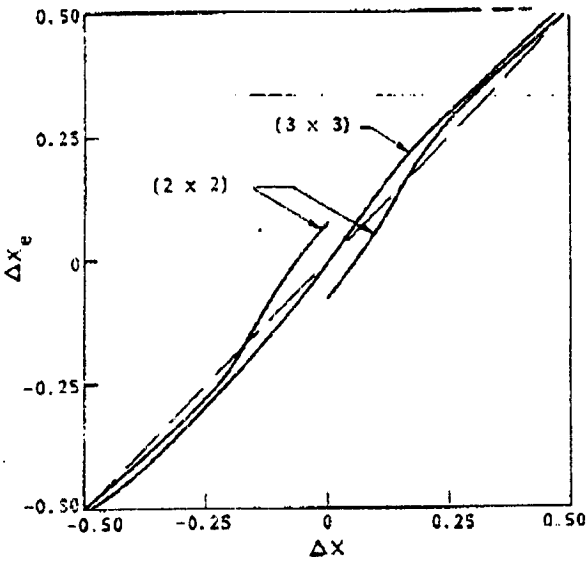

FIG. 1 ALGORITHM PREDICTION VERSUS ACTUAL OFFSET

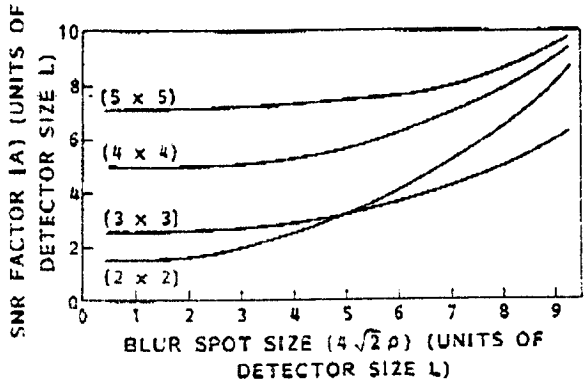

FIG. 2 SNR ERROR MULTIPLICATIVE FACTOR [$\bar{A}$] VERSUS BLUR SPOT SIZE

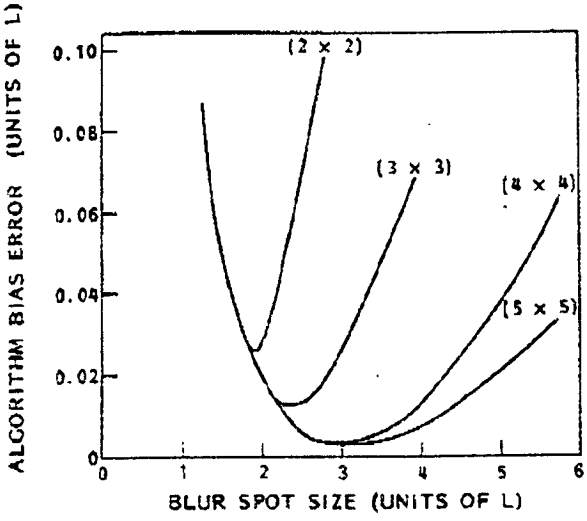

FIG. 3 ALGORITHM BIAS ERROR [$\bar{B}$] VERSUS BLUR SPOT SIZE

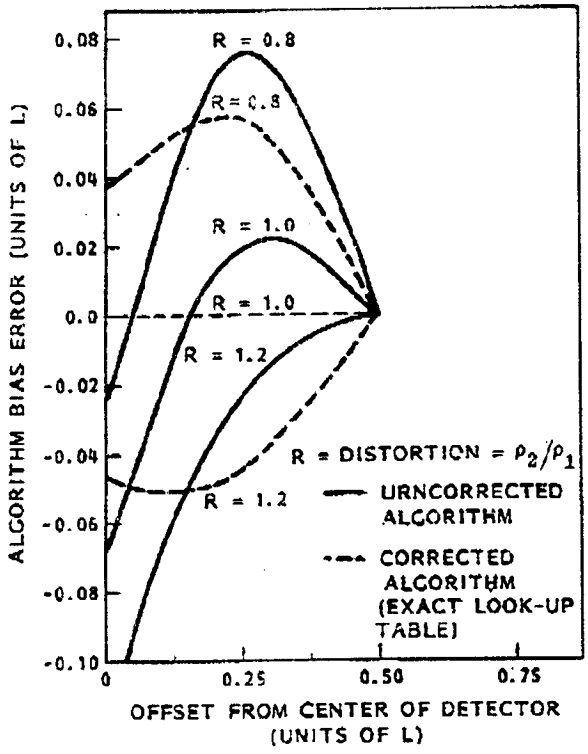

FIG. 4 CHANGE IN (2 x 2) ALGORITHM BIAS ERROR WITH DISTORTION

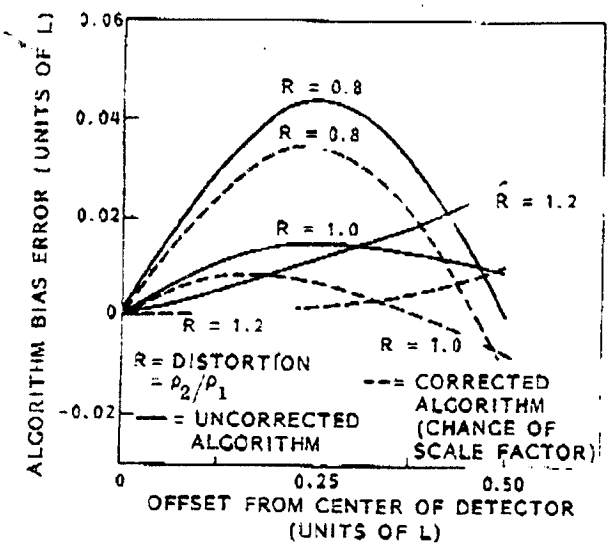

FIG. 5 CHANGE IN (3 x 3) ALGORITHM BIAS ERROR WITH DISTORTION

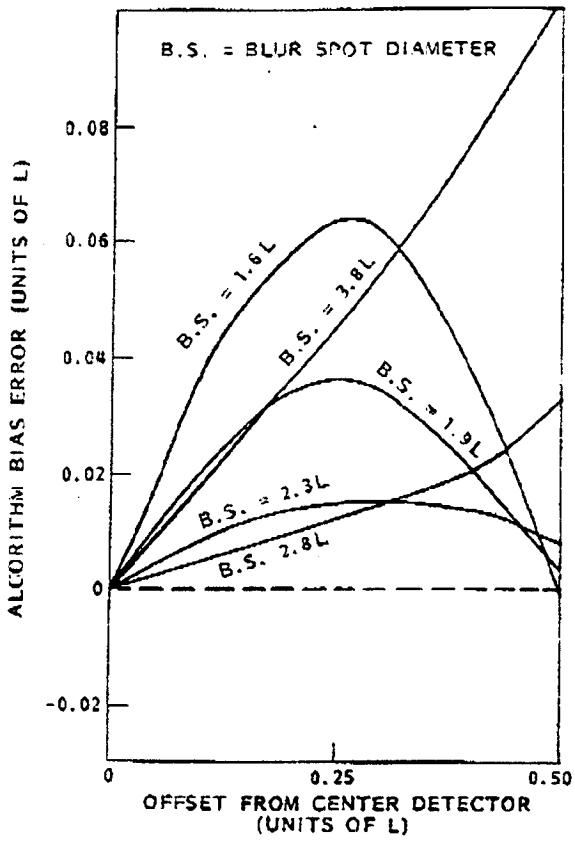

FIG. 6 (3 x 3) ALGORITHM BIAS ERROR VERSUS OFFSET FOR SEVERAL BLUR SPOT SIZES

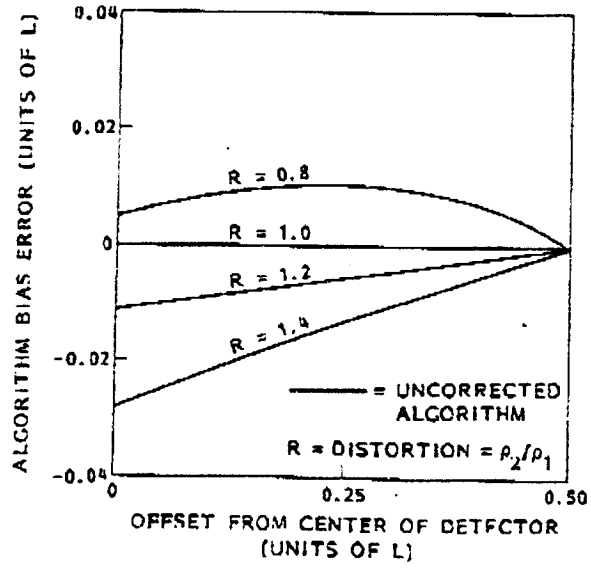

FIG. 7 CHANGE IN (4 x 4) ALGORITHM BIAS ERROR WITH DISTORTION

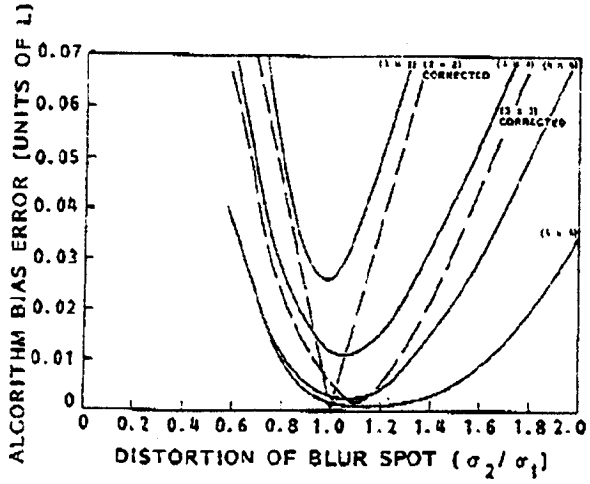

FIG. 8 EFFECT ON THE ALGORITHM BIAS ERROR OF BLUR SPOT DISTORTION

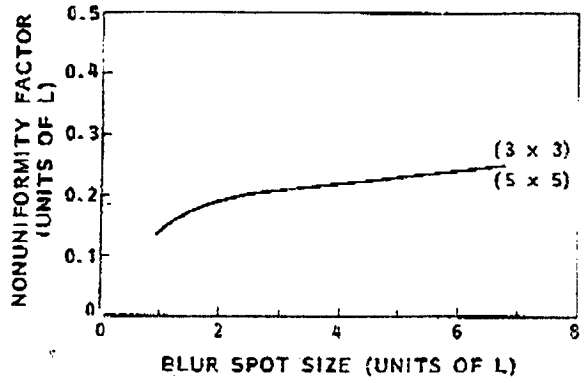

FIG. 9 NONUNIFORMITY FACTOR $\bar{D}$

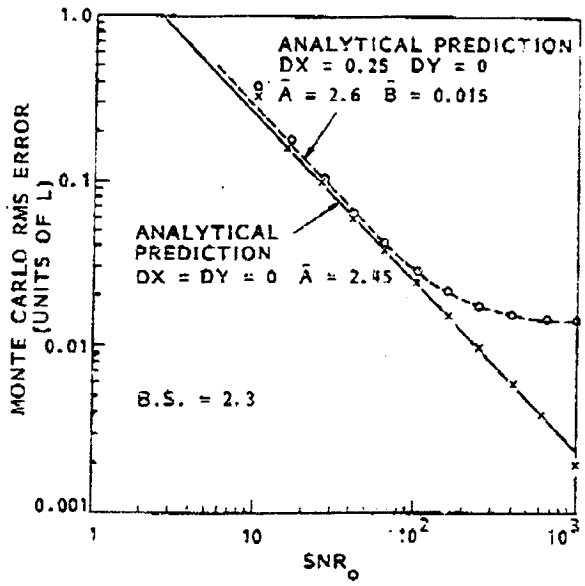

FIG. 10 SAMPLE MONTE CARLO RESULTS AS A FUNCTION OF SNR_o

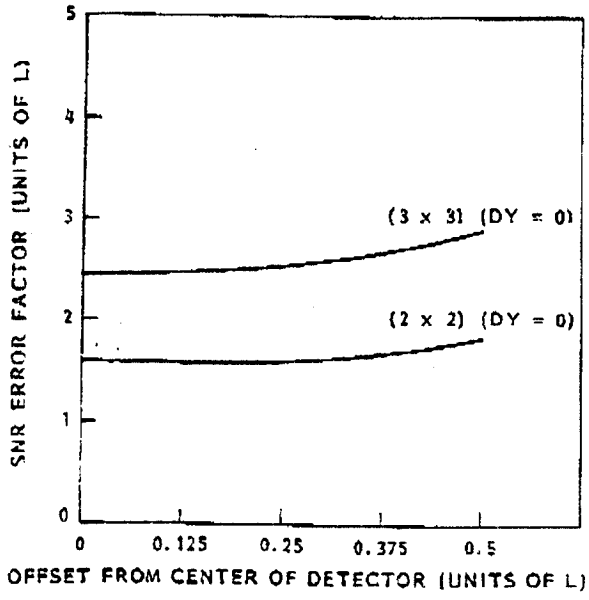

FIG. 11 OFFSET DEPENDENCE OF ERROR FACTOR (ALONG 1 AXIS)

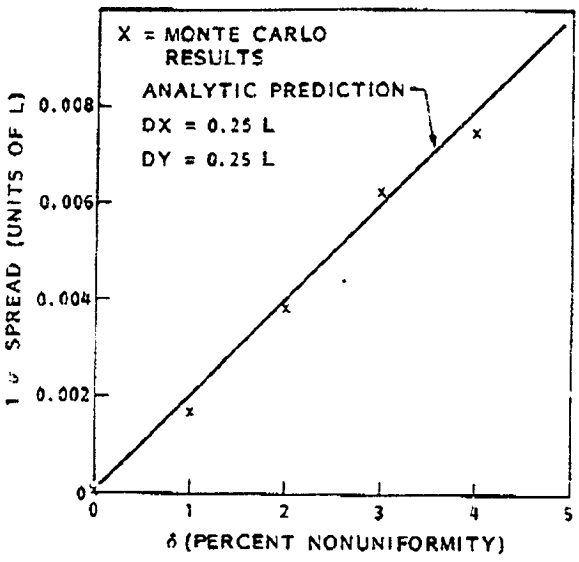

FIG. 12 SPREAD OF ALGORITHM BIAS $\bar{B}$ DUE TO RESPONSIVITY NONUNIFORMITY